Front. Mater. Sci. 2024, 18(1): 240675
https://doi.org/10.1007/s11706-024-0675-y

RESEARCH ARTICLE

Carbon nanotubes-reinforced polylactic acid/hydroxyapatite porous scaffolds for bone tissue engineering

Weiwei Lan[1*], Mingbo Wang[2*], Zhenjun Lv[1], Jun Li[1], Fuying Chen[1], Ziwei Liang[1,3], Di Huang (✉)[1,3], Xiaochun Wei[4], and Weiyi Chen[1,3]

1 Research Center for Nano-Biomaterials & Regenerative Medicine, Department of Biomedical Engineering, College of Biomedical Engineering, Taiyuan University of Technology, Taiyuan 030024, China
2 Guangdong Engineering Technology Research Center of Implantable Medical Polymer, Shenzhen Lando Biomaterials Co., Ltd., Shenzhen 518107, China
3 Shanxi-Zheda Institute of Advanced Materials and Chemical Engineering, Taiyuan 030060, China
4 Department of Orthopaedics, The Second Hospital of Shanxi Medical University, Taiyuan 030001, China

ABSTRACT: In the field of bone defect repair, critical requirements for favorable cytocompatibility and optimal mechanical properties have propelled research efforts towards the development of composite materials. In this study, carbon nanotubes/polylactic acid/hydroxyapatite (CNTs/PLA/HA) scaffolds with different contents (0.5, 1, 1.5 and 2 wt.%) of CNTs were prepared by the thermally induced phase separation (TIPS) method. The results revealed that the composite scaffolds had uniform pores with high porosities over 68% and high through performances. The addition of CNTs significantly enhanced the mechanical properties of resulted PLA/HA, in which the 1.5 wt.% CNTs/PLA/HA composite scaffold demonstrated the optimum mechanical behaviors with the bending elastic modulus of (868.5 ± 12.34) MPa, the tensile elastic modulus of (209.51 ± 12.73) MPa, and the tensile strength of (3.26 ± 0.61) MPa. Furthermore, L929 cells on the 1.5 wt.% CNTs/PLA/HA scaffold displayed good spreading performance and favorable cytocompatibility. Therefore, it is expected that the 1.5 wt.% CNTs/PLA/HA scaffold has potential applications in bone tissue engineering.

KEYWORDS: CNTs/PLA/HA scaffold; TIPS method; mechanical property; bone tissue engineering

Contents

Received August 29, 2023; accepted December 20, 2023

E-mail: huangjw2067@163.com

∗ W.L. and M.W. contributed equally to this work and should be regarded as co-first authors.

1 Introduction

Natural bone tissues owning the complex multiscale structure consist of organic and inorganic substances [1], which provide the human body with sufficient mechanical supporting, mineral storage, and internal protection. In recent years, the research about bone regeneration has been driven by the need for repair of bone defects and bone loss resulting from infections, tumors, or traumas [2–4]. Although natural bones show self-repair ability, the larger bone defects beyond their self-recovery still need surgical intervention. Unfortunately, current surgical approaches, such as autografts and allografts, are far from ideal and merely serve as temporary solutions due to the existence of issues including immune responses, donor-site complications, and limited donor availability [5–11].

The advancement of bone tissue engineering has led to the emergence of bone composite scaffolds as a promising alternative for the treatment of bone defects, particularly in larger-scale cases. Bioceramic materials, including hydroxyapatite (HA) and tricalcium phosphate (TCP), have recently gained considerable attention as suitable substitutes for bone-related tissue engineering [12–15]. Particularly, HA was extensively adopted in the fabrication of bone repair scaffolds for extraordinary bioactivity, biocompatibility, and bone conductibility [12,16–17]. During the degradation of HA *in vivo*, the Ca and P ions generated could be directly involved in the remodeling of new bones, and some researches even confirmed the participation of Ca^{2+} in the regulation of many physiological functions in the human body [18]. However, pure HA scaffolds suffered from brittleness, low toughness, and slow degradation, thereby significantly limiting their application in the bone defect reconstruction [16]. To address such limitations, the incorporation of polymers, such as collagen, chitosan (CS), polyvinyl alcohol (PVA), and polylactic acid (PLA) whether they are natural or synthetic, has been explored to enhance the toughness of HA scaffolds [19–22].

As an extensively applied material, PLA has gained wide attention in serving as medical devices, such as scaffolds, drug delivery systems, and tissue engineering, owing to its good biocompatibility, favorable mechanical capability, high biodegradability, and nontoxicity of degradation products [23–24]. However, pure PLA has some drawbacks as well, namely, poor bioactivity, high hydrophobicity, and long degradation time. Therefore, numerous studies have been focused on improving the bioactivity of PLA with surface engineering or bioactive addition to be suited for tissue engineering [25]. Among all these materials, PLA with bioceramics showed better appropriateness for bone tissue engineering. It was proven that TCP could not only improve the PLA surface wettability, but also increase the cell attachment [12,25]. Meanwhile, PLA/HA porous scaffolds had superior osteoinductivity, improved mechanical property, excellent biocompatibility, and good absorbability [26]. Although TCP and HA could help to buffer inflammatory responses, diminish harmful effects of the degradation of polymers, and improve cell attachments, the weak interfacial adhesion between HA/TCP particles and the PLA matrix as well as the agglomeration of HA/TCP particles in the matrix might hinder their effectiveness in load-bearing areas [27–28]. This issue primarily arises from the significant chemical dissimilarity between HA and PLA, resulting in a weak bonding at the composite interface. Furthermore, the mechanical performances of PLA/HA are still inadequate when compared to natural bone tissues. Therefore, it is urgent to further improve the mechanical capabilities of PLA/HA porous scaffolds with the intention of better meeting the requirements from applications in bone tissue engineering.

Carbon nanotubes (CNTs) possess desirable thermal conductivity, electrical conductivity, and mechanical properties, making them highly valuable for tissue engineering applications [29–32]. The incorporation of CNTs into polymers has been extensively utilized to enhance the modulus, to improve the interfacial adhesion, and even to generate novel mechanical properties of the resulting composites [33–34]. The mechanisms on how CNTs enhanced the mechanical properties of composite scaffolds were multifaceted involving various aspects such as the ability of CNTs to enhance the load transfer capability and improve the interfacial bonding between inorganic dispersions and organic bodies. CNTs could

enhance the cell–cell interactions, adhesion, proliferation, and osteogenic differentiation, contributing to improved bone growth [31]. However, it is important to note that CNTs have a tendency for agglomeration due to their structures with high aspect ratios and interactions by intrinsic van der Waals forces. Once the agglomeration of CNTs is induced, the dispersion of them within the composite system becomes more challenging, which has negative impacts on the desired properties [5]. Therefore, it is crucial to determine the appropriate concentration of CNTs in the composite scaffold for their effective dispersion and beneficial effects.

Up to now, it still remains a challenge of developing orthopedic materials that combine excellent biocompatibility and biomimetic pore size structure. Herein, the properties of PLA/HA porous scaffolds were improved by the addition of CNTs with different contents (0.5, 1, 1.5, and 2 wt.%). The morphology, porosity, mechanical properties and degradation performances of CNTs/PLA/HA porous scaffolds were revealed. Besides, the effect of CNTs on cytocompatibility was also investigated by seeding L929 cells onto the surface of composite scaffolds.

2 Materials and methods

2.1 Materials

HA was prepared by the chemical precipitation method [12]. PLA and CNTs were purchased from Cool Seoul Biological (China) and Aladdin (China), respectively. Dichloromethane was purchased from Tianjin Fuyu Fine Chemical Co., Ltd. (China). Dulbecco's modified Eagle's medium/Nutrient Mixture F-12 (DMEM/F12) was obtained from Hyclone (USA). Fetal bovine serum (FBS) was purchased from Gibco (USA). Other chemicals were purchased from Puxing Chemical Co., Ltd. (Taiyuan, China). All reagents were of analytical grade.

2.2 Preparation of porous scaffolds

In this work, the thermally induced phase separation (TIPS) method was used to prepare porous scaffolds [35–36]. TIPS is a thermally delimited technique in which a homogeneous polymer-solvent solution becomes a polymer-rich phase, typically by exposing the solution to a dilute phase of the polymer [36]. As shown in Fig. 1, the whole system consisted of three parts: a heating device (water bath), a heat conducting device (beaker), and a mixture slurry. Specifically, PLA was added into dichloromethane and stirred until completely dissolved (5 wt.%) at room temperature. Then, HA powder was added into the PLA solution by continuous stirring until it was completely dispersed, forming a milky-white suspension of PLA/HA with the mass ratio of 7:3. In the pre-experiment, we fabricated PLA/HA scaffolds with different mass ratios (8:2, 7:3, and 6:4) and selected PLA/HA with the mass ratio of 7:3 in this study considering its enhanced mechanical strength and suitable structure. Immediately, different amounts of CNTs were added into the PLA/HA solutions to make the CNT concentrations reach 0.5, 1, 1.5, and 2 wt.% separately in the mixed systems, followed by the ultrasound treatment for 30 min to disperse CNTs homogeneously. Subsequently, the mixtures were allowed to evaporate in water bath at 95 °C. After complete evaporation of the solvent (dichloromethane), the composite porous scaffolds were therefore formed.

2.3 Physicochemical properties of scaffolds

The inner-structures of PLA/HA and CNTs/PLA/HA scaffolds were observed by scanning electron microscopy (SEM) with a JSM-7100F instrument (JEOL, Japan), following the gold sputtering onto each sample.

Fourier-transform infrared spectroscopy (FTIR) patterns of PLA/HA and CNTs/PLA/HA porous scaffolds were recorded on a FT-IR spectrometer (Thermo Fisher Scientific, United States) in the attenuated total reflectance (ATR) mode within the wavenumber range of 4000–400 cm^{-1}.

X-ray diffraction (XRD) was performed on PLA/HA and CNTs/PLA/HA porous scaffolds by an X-ray diffractometer (Y-2000A, China) operated at 40 kV and 35 mA. The scan rate was 0.05(°)·s^{-1} with the 2θ value ranging from 10° to 80°.

2.4 Porosity analysis

The porosity of each fabricated scaffold was determined according to the density method. In brief, the theoretical density (ρ) of various types of porous scaffolds was calculated based on the solvent proportion in the porous scaffold. Then, the actual density (ρ_1) of the sample holder was calculated by weighing the actual mass (M)

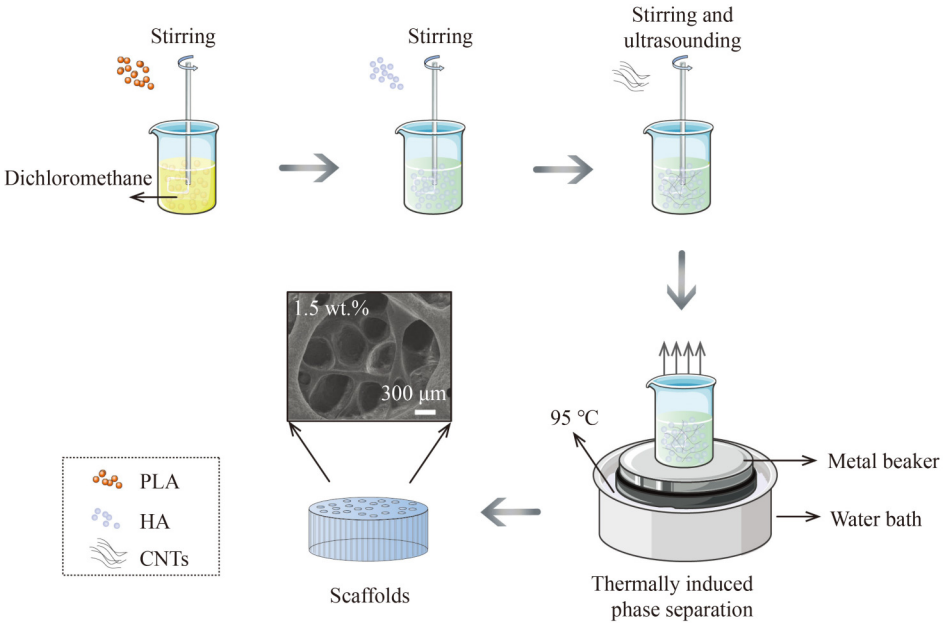

Fig. 1 Schematic diagram of the scaffold preparation.

and estimating the actual body (V) of various types of porous scaffolds after drying. The porosity (φ) of each scaffold was then obtained by the equation as follows:

$$\varphi/\% = \frac{|\rho - \rho_1|}{\rho} \times 100 \quad (1)$$

2.5 Mechanical property testing

PLA/HA and CNTs/PLA/HA porous scaffolds were subjected to a mechanical test to determine mechanical properties, including bending properties and tensile properties, with a universal testing machine (Instron 5544, USA). The specimens (n = 5) were cut into uniform rectangular shapes (30 mm in length, 1 mm in width, and 0.1 mm in thickness) and then placed on a platform that measured bending performance and tensile properties. The stretching rate was 10 mm·min^{-1} and the bending loading rate was 3.5 mm·min^{-1}. The bending modulus of elasticity and the bending fracture energy were calculated based on data of the load–displacement relation from the three-point bending test, while the tensile elastic modulus and the tensile strength were obtained from the stress–strain curve of the stretching process.

2.6 *In vitro* degradation experiments

To evaluate the degradation rates of scaffolds under body fluid-like conditions, PLA/HA and CNTs/PLA/HA porous scaffolds (20 mm in length, 5 mm in width, and 0.1 mm in thickness) were weighed (W_1) and kept in small centrifuge tubes filled with 3 mL of phosphate buffer solution (PBS; pH = 7.4), followed by culturing on an orbital shaker at 37 °C for different durations (14 and 21 d). After each incubation process, the samples were washed for several times by deionized water and weighted (W_2) after drying for 48 h. Finally, the *in vitro* degradation ratio (η) was expressed as the weight loss ratio by the following equation:

$$\eta/\% = \frac{W_1 - W_2}{W_1} \times 100 \quad (2)$$

2.7 *In vitro* cell analysis

All scaffolds were sterilized by an autoclave, and then they were washed for three times in DMEM/F12 before seeding. L929 cells were cultured at 37 °C under a humidified environment with 5% CO_2 in DMEM/F12 that contained 10% FBS and 1% antibiotic/antimycotic compounds. Afterwards, they were digested with 0.05% trypsin/EDTA and suspended in fresh media. To observe the cell attachment on scaffolds, pre-treated scaffolds were placed at the bottom of a 24-well cell-culture plate, followed by seeding of the cell suspension onto them.

The morphology of cells on scaffolds was separately observed by SEM after seeding for 3 and 5 d. Briefly, the scaffolds with cells were transferred from the 24-well

plate, washed by phosphate-buffered saline (PBS) for three times, and fixed with 2.5% glutaraldehyde for 40 min. After the scaffolds were washed thrice in PBS again, they were separately dehydrated in ethanol solutions with different concentrations (30%, 50%, 70%, 90%, 95%, and 100%). Finally, the cell-seeded scaffolds coated with a thin layer of gold were prepared for SEM observation.

The proliferation of L929 cells on different scaffolds was further evaluated by the MTT test at various time points after separately seeding for 1, 3, and 5 d (n = 5). L929 cells with the density of 2 × 10^4 cells/well were seeded onto each scaffold and cultured in regular DMEM/F12 supplemented with 10% FBS and 1% antibiotic/antimycotic in the 24-well plate. At each time point, the culture medium was removed and replaced with the prepared MTT solution. After incubation for another 4 h, an aliquot of the solution in each well was transferred into a new 96-well plate, and the light absorbance at 595 nm was measured by a microplate reader (Bio-Rad iMark, USA).

2.8 Statistical analyses

All statistical analyses were performed using SPSS (IBM Corp., USA), and continuous variables were expressed as the mean ± standard deviation (SD). Statistical comparisons were carried out by using a one-way analysis of variance (ANOVA) followed by a Student's t-test. The level of significance was defined as $p < 0.05$.

3 Results and discussion

3.1 Morphology and structural properties of scaffolds

It is of great importance to fabricate porous scaffolds with interconnected porosity and large pores for bone tissue engineering, which should be conducive to the migration of bone cells, the regeneration of bone tissues, and the formation of new bones *in vitro* and *in vivo* [37–39]. Besides, the effect of nanoscale pore-size distribution (PSD) can further improve both the transport of body fluids and the interaction between cells and scaffolds in the whole fabrication process of scaffolds [40–41]. In this work, porous scaffolds were prepared by the TIPS method. Figure 2 shows SEM images under two magnifications of CNTs/PLA/HA porous scaffolds containing different contents of CNTs, from which it is seen that each sample has the porous structure with a double PSD, and there is no apparent difference in the PSD with the addition of CNTs. Meanwhile, the uniform and unidirectional porous inner structure is also presented, which should form during the fabrication process. Specifically, a beaker containing the composite slurry was heated from the bottom in the water bath, resulting in the decomposition of dichloromethane in slurry from the liquid phase to the gas phase. During the phase-separation process, the gasification endothermic reaction made the beaker temperature gradually lowered from bottom to top, leading to the formation of temperature gradient in the vertical direction. Thus, the formation of pores was induced along the bottom to the top of the mixed slurry,

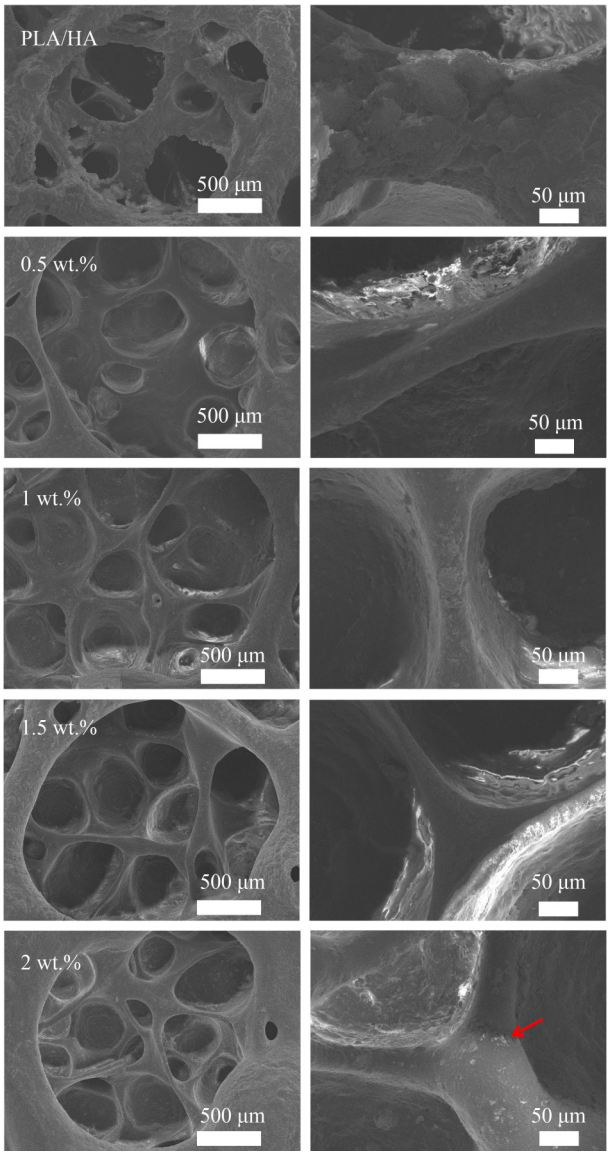

Fig. 2 SEM images of each scaffold under different magnifications.

forming a one-way foam and subsequently a unidirectional porous support [35]. In addition, a small amount of aggregated HA appeared at the interface between pores (arrow in Fig. 2) when the content of CNTs was 2 wt.%, which might be related to the intense interaction between CNTs and HA nanoparticles.

3.2 FTIR analyses

FTIR spectra of all samples are presented in Fig. 3(a). It is observed that both PLA/HA and CNTs/PLA/HA scaffolds have the same characteristic absorption peak positions. The appearance of peaks corresponding to C−O−C and C=O stretching vibrations at 1090, 1189, and 1750 cm^{-1}, P−O asymmetric contraction vibrations at 873, 963, and 1035 cm^{-1}, and −CH and −CH− stretching vibrations at 1460 and 2948–3010 cm^{-1} further reveals the good combination of PLA and HA. Compared with those for PLA/HA porous scaffolds, the addition of CNTs brings about a slight narrowness and lowness of absorption peaks for composite scaffolds, especially of peaks at 1751 cm^{-1}, corroborating the chemical interaction between –OH groups from different contents of CNTs and −COOH groups from PLA [42].

3.3 XRD analyses

Figure 3(b) shows XRD patterns of PLA/HA and 1.5 wt.% CNTs/PLA/HA porous scaffolds compared with that of pure HA powder. The results indicate that the addition of CNTs has no obvious effect on crystallization properties of the PLA/HA porous scaffold, since there are no new feature peaks and peak shift characteristics for the CNTs/PLA/HA porous scaffold except for some features of the peak widening.

3.4 Porosity analyses

The porosities of all porous scaffolds are revealed in Fig. 4. It is detected that increasing the content of CNTs results in the decrease of the porosity. In this study, the 2 wt.% CNTs/PLA/HA scaffold has the lowest porosity (i.e., 68.45% ± 0.50%), while there is no significant difference among each group ($p > 0.05$). For all porous scaffolds, their porosities are high enough to meet the requirements for bone tissue engineering.

3.5 Mechanical properties of scaffolds

There are three essential elements in bone tissue engineering, namely cells, scaffolds, and bioactive factors, among which scaffolds are fundamental for supporting the long-term *in vivo* regeneration of defects. Many studies have proven that the mechanical properties of scaffolds are the key to directing cellular biological behaviors [43–44]. Figure 5 shows the results of bending and tensile tests on porous scaffolds with various contents of CNTs compared with that on the PLA/HA porous scaffold. It is detected that the introduction of CNTs into PLA/HA can improve the bending and tensile properties of the resulted porous scaffold to a large extent. Particularly, with the continuous increase of the CNT content, the bending and tensile properties of the porous scaffold are increased at first but decreased later. The optimum mechanical properties are obtained when the CNT content is 1.5 wt.% with the bending elastic modulus of (868.5 ± 12.34) MPa, the bending fracture energy of (0.10 ± 0.01) kJ, the tensile elastic modulus of (209.51 ± 12.73) MP, and the tensile strength of (3.26 ± 0.61) MPa. It is known that CNTs have attracted much attention owing to their unique properties such as high conductivity, large surface-to-volume ratio,

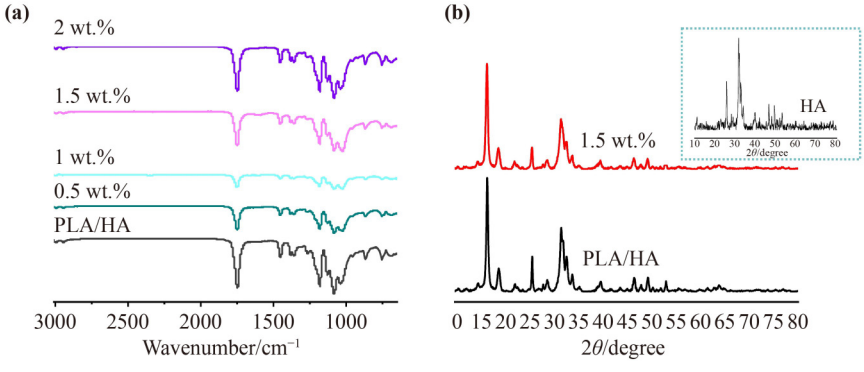

Fig. 3 (**a**) FTIR spectra of PLA/HA and CNTs/PLA/HA scaffolds (with different CNT concentrations of 0.5, 1, 1.5, and 2 wt.%). (**b**) XRD patterns of HA, PLA/HA, and 1.5 wt.% CNTs/PLA/HA.

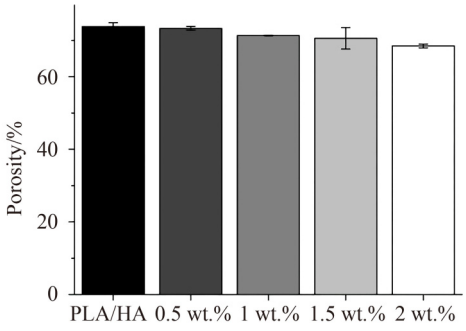

Fig. 4 The porosities of all scaffolds.

and special chemical activity [45]. As functional fillers, CNTs have been proposed to improve both mechanical and electrical properties of tissue engineering scaffolds [46]. The addition of a small amount of CNTs will improve the mechanical properties of the composite because CNTs can be uniformly dispersed into the scaffold and set as stress points when the construct is subject to dynamic loads. However, some related studies have also presented that the presence of a large amount of CNTs may cause uneven dispersion that damages the inner structure of the scaffold, having an adverse effect on its mechanical properties [32,47]. It can also be observed from Fig. 2 that when the CNT content reaches 2 wt.%, some HA and CNT agglomerations are formed.

Moreover, Fig. 6 shows fracture surfaces of the 1.5 wt.% CNTs/PLA/HA porous scaffold after separately bending and stretching. It is clear that both cross-sections of the scaffold were rough with a small amount of extension, revealing the overall trend of tough fractures which could withstand greater force.

3.6 Degradation performance *in vitro*

Figure 7(a) shows mass losses of PLA/HA and CNTs/PLA/HA scaffolds at different time points after degradation in PBS. It is seen that all samples, except for the 2 wt.% CNTs/PLA/HA scaffold, lost masses after degradation for 14 d. Meanwhile, compared with that of the PLA/HA sample, the degradation rates of all CNTs/PLA/HA scaffolds except for that with 2 wt.% CNTs became relatively slower. Specifically, the mass loss of the PLA/HA scaffold reached 15.45% ± 1.25%, while CNTs/PLA/HA scaffolds with the CNTs contents of 0.5, 1, and 1.5 wt.% had lower mass losses between 5% and 7% (with significant difference, $p < 0.05$), which may be related to the enhanced interfacial fastness of the composites with CNTs [48]. Although previous SEM images in Fig. 2 confirmed that the rise of the CNTs content made no significant change in the pore size of scaffolds, the results in Fig. 4 indicated that there was a decrease in porosity (with no significant difference),

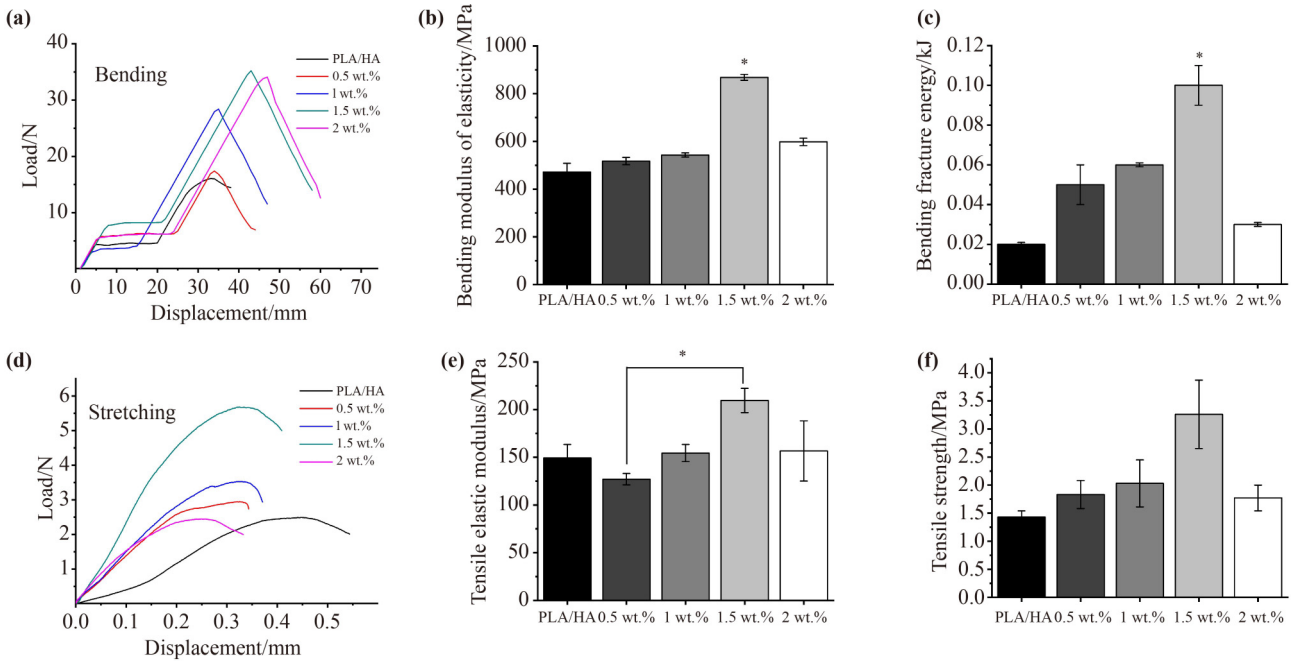

Fig. 5 Mechanical properties of each scaffold: (**a**) the bending load–displacement figure; (**b**) the bending modulus of each scaffold (*$p < 0.05$); (**c**) the bending fracture energy of each scaffold (*$p < 0.05$); (**d**) the stretching load–displacement figure; (**e**) the tensile modulus of each scaffold (*$p < 0.05$); (**f**) the tensile strength of each scaffold.

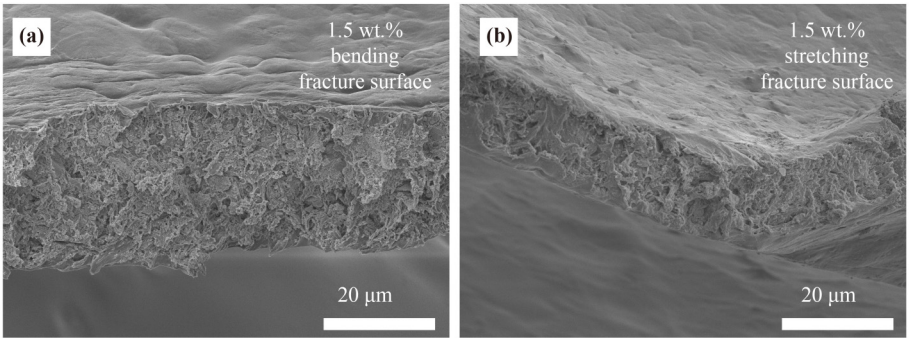

Fig. 6 Fracture surfaces of the 1.5 wt.% CNTs/PLA/HA porous scaffold: (**a**) the bending section; (**b**) the stretching section.

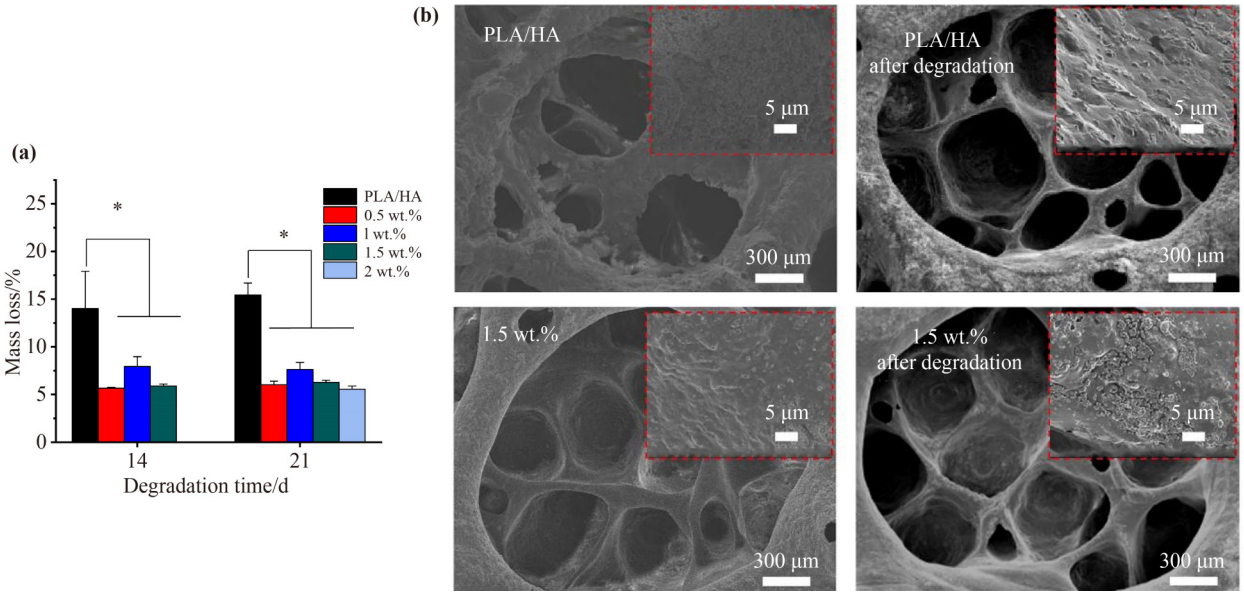

Fig. 7 Degradation analyses on scaffolds: (**a**) mass losses of scaffolds at different degradation time points (*p < 0.05); (**b**) SEM images of PLA/HA and 1.5 wt.% CNTs/PLA/HA porous scaffolds before and after the degradation for 21 d.

signifying that the addition of CNTs make scaffolds denser. It is believed that the addition of HA would enhance the binding strength of the scaffold interface, while the involvement of CNTs would further improve the binding strength causing the composites hardly decomposed into small-molecular-weight substances [49].

Figure 7(b) shows SEM images of PLA/HA and 1.5 wt.% CNTs/PLA/HA porous scaffolds before and after the degradation for 21 d, reflecting the change of the surface morphology. In the case of the PLA/HA porous scaffold, compared with the one before degradation, the post-degraded sample had larger pore sizes and much more narrowness in the intervening space, accompanied by the smoother surface owing to the decrease of the HA agglomeration. Although the 1.5 wt.% CNTs/PLA/HA porous scaffold also had larger pore sizes after degradation, its surface became rougher, contrary to that of the post-degraded PLA/HA porous scaffold. Meanwhile, the visible "grain", caused by the degradation of HA and PLA, appeared, resulting in the exposure of undegraded CNTs. In conclusion, the addition of CNTs significantly slowed down the degradation of PLA/HA.

3.7 *In vitro* cytocompatibility study

According to above tests, we selected 1.5 wt.% CNTs/PLA/HA as our experiment group to conduct the cytocompatibility study. The results showed that the MTT absorbance of L929 cells seeded on each scaffold increased with the prolonging of culturing time (Fig. 8(a)). Compared with that of the PLA/HA scaffold, cells on the CNTs/PLA/HA scaffold showed a slightly lower proliferation rate, while there was no statistically significant difference. It was clearly shown that cells

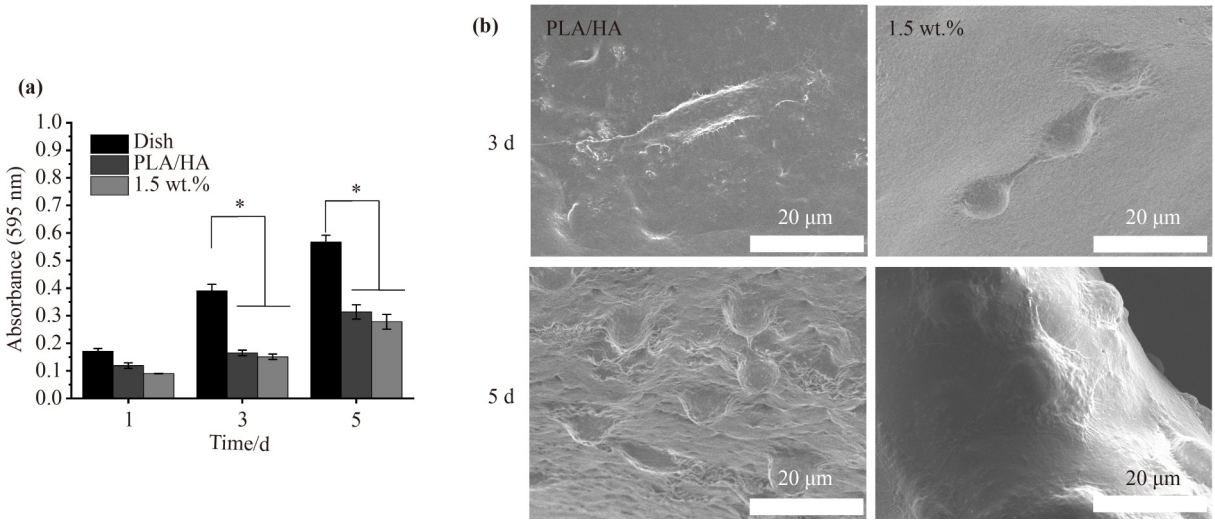

Fig. 8 Proliferation rates and spreading performances of L929 cells on each scaffold: (**a**) proliferation rates of L929 cells seeded *in vitro* on each scaffold at different time points (*$p < 0.05$); (**b**) SEM images of L929 cells *in vitro* on each scaffold at different culturing time points.

cultured on dishes had the highest proliferation rate ($p < 0.05$), which might be due to the difference of cell culturing microenvironments.

To further observe the spreading behavior of L929 cells on each scaffold, SEM was conducted. It was seen from Fig. 8(b) that there were core- and spindle-shaped L929 cells on each scaffold, and the addition of CNTs had no significant influence on the adhesion and spreading of cells. It was apparent that the spreading morphology of L929 cells on the 1.5 wt.% CNTs/PLA/HA scaffold became broader with more numerous filopodia after culturing for 5 d, which was the evidence that the 1.5 wt.% CNTs/PLA/HA scaffold could facilitate cell spreading.

There were numerous studies which proved that cells cultured on two-dimensional (2D) dishes presented better proliferation than those on three-dimensional (3D) scaffolds [50]. However, it was confirmed that 3D culture scaffolds were more similar to the cells' natural environment, and cells cultured on 2D dishes would loss function phenotype and produce less extracellular matrix [51]. Furthermore, some researches have proven that CNTs possess the potential to promote the bone formation because of their similar structure with that of natural bones [52–53].

4 Conclusion

In this study, CNTs were incorporated into PLA/HA scaffolds by a simple TIPS technique to achieve improved mechanical properties and good cytocompatibility. The effects of the CNT content on fabricated scaffolds were explored. According to results from FTIR and XRD, there was no effect on the crystallinity of PLA/HA porous scaffolds and the binding of characteristic groups with the addition of CNTs. There was also no obvious difference in PSD and porosity after adding CNTs. However, the incorporation of CNTs into PLA/HA remarkably enhanced the mechanical properties of the resulted composite, specifically for 1.5 wt.% CNTs/PLA/HA, and L929 cells on the 1.5 wt.% CNTs/PLA/HA scaffold revealed good spreading performance and favorable cytocompatibility. This study confirms that the incorporation of CNTs can dramatically enhance the mechanical properties of PLA/HA scaffolds without affecting their own structures and cytocompatibility, providing new potential applications in bone tissue engineering.

Authors' contributions Weiwei Lan wrote the manuscript, analyzed the data, plotted the graphs, and provided funding for the experiments. Mingbo Wang wrote and revised the manuscript. Zhenjun Lv, Jun Li, and Fuying Chen operated the experiments. Ziwei Liang and Xiaochun Wei revised and checked the manuscript. Weiyi Chen provided funding for the experiments. Di Huang conceptualized and supervised the experiment, obtained funding, and managed the project.

Declaration of competing interests The authors declare that they have no known competing financial interests or personal relationships that could have appeared to influence the work reported in this paper.

Acknowledgements This work was supported by the National Natural Science Foundation of China (Grant Nos. 12202302, 12272253, and

82103147). The support of the Fund Program for the Scientific Activities of Selected Returned Overseas Professionals in Shanxi Province (Grant No. 20220006) was also acknowledged with gratitude.

References

[1] Hong M H, Lee J H, Jung H S, et al. Biomineralization of bone tissue: calcium phosphate-based inorganics in collagen fibrillar organic matrices. Biomaterials Research, 2022, 26(1): 42

[2] Migliorini F, La Padula G, Torsiello E, et al. Strategies for large bone defect reconstruction after trauma, infections or tumour excision: a comprehensive review of the literature. European Journal of Medical Research, 2021, 26(1): 118

[3] Li C, Lv H, Du Y, et al. Biologically modified implantation as therapeutic bioabsorbable materials for bone defect repair. Regenerative Therapy, 2022, 19: 9–23

[4] Xu C, Kang Y, Guan S, et al. Iron-based metal–organic framework as a dual cooperative release system for enhanced vascularization and bone regeneration. Chinese Chemical Letters, 2023, 34(5): 107825

[5] Lan W, Xu M, Qin M, et al. Physicochemical properties and biocompatibility of the bi-layer polyvinyl alcohol-based hydrogel for osteochondral tissue engineering. Materials & Design, 2021, 204: 109652

[6] Huey D J, Hu J C, Athanasiou K A. Unlike bone, cartilage regeneration remains elusive. Science, 2012, 338(6109): 917–921

[7] Cui Y, Liu H, Tian Y, et al. Dual-functional composite scaffolds for inhibiting infection and promoting bone regeneration. Materials Today: Bio, 2022, 16: 100409

[8] Levingstone T J, Matsiko A, Dickson G R, et al. A biomimetic multi-layered collagen-based scaffold for osteochondral repair. Acta Biomaterialia, 2014, 10(5): 1996–2004

[9] Zhang J, Tong D, Song H, et al. Osteoimmunity-regulating biomimetically hierarchical scaffold for augmented bone regeneration. Advanced Materials, 2022, 34(36): 2202044

[10] Peng Y, Zhuang Y, Liu Y, et al. Bioinspired gradient scaffolds for osteochondral tissue engineering. Exploration, 2023, 3(4): 20210043

[11] Peng Y, Zhuang Y, Zhang Y, et al. Dynamically adaptive scaffolds for cartilage tissue engineering. MedComm – Biomaterials and Applications, 2023, 2(3): e49

[12] Huang D, Niu L, Wei Y, et al. Interfacial and biological properties of the gradient coating on polyamide substrate for bone substitute. Journal of the Royal Society Interface, 2014, 11(99): 20140101

[13] Zerankeshi M M, Mofakhami S, Salahinejad E. 3D porous HA/TCP composite scaffolds for bone tissue engineering. Ceramics International, 2022, 48(16): 22647–22663

[14] Zou Z, Wang L, Zhou Z, et al. Simultaneous incorporation of PTH(1-34) and nano-hydroxyapatite into chitosan/alginate hydrogels for efficient bone regeneration. Bioactive Materials, 2021, 6(6): 1839–1851

[15] Wang Q, Luan J, Zhao Z, et al. Dentin-desensitizing biomaterials. Chinese Chemical Letters, 2023, 34(8): 108060

[16] Yan C, Ma G, Chen A, et al. Additive manufacturing of hydroxyapatite and its composite materials: a review. Journal of Micromechanics and Molecular Physics, 2020, 5(3): 2030002

[17] Sri A K, Arthi C, Neya N R, et al. Nano-hydroxyapatite/collagen composite as scaffold material for bone regeneration. Biomedical Materials, 2023, 18(3): 032002

[18] Zheng P, Ding J. Calcium ion nanomodulators for mitochondria-targeted multimodal cancer therapy. Asian Journal of Pharmaceutical Sciences, 2022, 17(1): 1–3

[19] Tian Z, Guo Y, Yang X, et al. Nano calcium-deficient hydroxyapatite/*O*-carboxymethyl chitosan-$CaCl_2$ microspheres loaded with rhein for bone defect repair. Journal of Bionics Engineering, 2022, 19(4): 1087–1099

[20] Zhang B, Wang L, Song P, et al. 3D printed bone tissue regenerative PLA/HA scaffolds with comprehensive performance optimizations. Materials & Design, 2021, 201: 109490

[21] Hartatiek H, Nasikhudin N, Putra A A D, et al. Study of surface morphology and porosity of composite scaffold nanofiber PVA/CS/HA with electrospinning method. Journal of Physical Science and Engineering, 2021, 6(1): 26–32

[22] Yu L, Rowe D W, Perera I P, et al. Intrafibrillar mineralized collagen–hydroxyapatite-based scaffolds for bone regeneration. ACS Applied Materials & Interfaces, 2020, 12(16): 18235–18249

[23] Osman M A, Virgilio N, Rouabhia M, et al. Polylactic acid (PLA) foaming: design of experiments for cell size control. Materials Sciences and Applications, 2022, 13(2): 63–77

[24] Surisaeng J, Kanabenja W, Passornraprasit N, et al. Polyhydroxybutyrate/polylactic acid blends: an alternative feedstock for 3D printed bone scaffold model. Journal of Physics: Conference Series, 2022, 2175(1): 012021

[25] Salamanca E, Tsao T C, Hseuh H W, et al. Fabrication of polylactic acid/β-tricalcium phosphate FDM 3D printing fiber to enhance osteoblastic-like cell performance. Frontiers in Materials, 2021, 8: 683706

[26] Akindoyo J O, Beg M D H, Ghazali S, et al. Synergized high-load bearing bone replacement composite from poly(lactic acid) reinforced with hydroxyapatite/glass fiber hybrid filler — mechanical and dynamic mechanical properties. Polymer Composites, 2021, 42(1): 57–69

[27] Ko H S, Lee S, Lee D, et al. Mechanical properties and bioactivity of poly(lactic acid) composites containing

poly(glycolic acid) fiber and hydroxyapatite particles. Nanomaterials, 2021, 11(1): 249

[28] Ko H S, Lee S, Jho J Y. Synthesis and modification of hydroxyapatite nanofiber for poly(lactic acid) composites with enhanced mechanical strength and bioactivity. Nanomaterials, 2021, 11(1): 213

[29] Zhao X, Chen X, Gui Z, et al. Carbon fiber reinforced hydroxyapatite composites with excellent mechanical properties and biological activities prepared by spark plasma sintering. Ceramics International, 2020, 46(17): 27446–27456

[30] Zhao X, Yang Z, Liu Q, et al. Potential load-bearing bone substitution material: carbon-fiber-reinforced magnesium-doped hydroxyapatite composites with excellent mechanical performance and tailored biological properties. ACS Biomaterials Science & Engineering, 2022, 8(2): 921–938

[31] Arumugam S, Ju Y. Carbon nanotubes reinforced with natural/synthetic polymers to mimic the extracellular matrices of bone — a review. Materials Today: Chemistry, 2021, 20: 100420

[32] Xu J, Xie Y, Zhang H, et al. Fabrication of PLGA/MWNTs composite electrospun fibrous scaffolds for improved myogenic differentiation of C2C12 cells. Colloids and Surfaces B: Biointerfaces, 2014, 123: 907–915

[33] Robert C, Thitasiri W B, Mamalis D, et al. Improving through-thickness conductivity of carbon fiber reinforced polymer using carbon nanotube/polyethylenimine at the interlaminar region. Journal of Applied Polymer Science, 2021, 138(5): e49749

[34] Salahuddin B, Faisal S N, Baigh T A, et al. Carbonaceous materials coated carbon fibre reinforced polymer matrix composites. Polymers, 2021, 13(16): 2771

[35] Cao Y, Han W, Pu Z, et al. Fabrication of hierarchically porous superhydrophilic polycaprolactone monolith based on nonsolvent-thermally induced phase separation. RSC Advances, 2020, 10(44): 26319–26325

[36] Wang H, Zuo Y, Zou Q, et al. Nano-hydroxyapatite/ polyamide66 composite tissue-engineering scaffolds with anisotropy in morphology and mechanical behaviors. Journal of Polymer Science Part A: Polymer Chemistry, 2009, 47(3): 658–669

[37] Radhakrishnan J, Muthuraj M, Gandham G S P D, et al. Nanohydroxyapatite–protein interface in composite sintered scaffold influences bone regeneration in rabbit ulnar segmental defect. Journal of Materials Science: Materials in Medicine, 2022, 33(4): 36

[38] Gómez-Cerezo M N, Peña J, Ivanovski S, et al. Multiscale porosity in mesoporous bioglass 3D-printed scaffolds for bone regeneration. Materials Science and Engineering C, 2021, 120: 111706

[39] Guastaferro M, Baldino L, Cardea S, et al. Supercritical processing of PCL and PCL–PEG blends to produce improved PCL-based porous scaffolds. Journal of Supercritical Fluids, 2022, 186: 105611

[40] Zhu L, Luo D, Liu Y. Effect of the nano/microscale structure of biomaterial scaffolds on bone regeneration. International Journal of Oral Science, 2020, 12(1): 6

[41] Wähnert D, Greiner J, Brianza S, et al. Strategies to improve bone healing: innovative surgical implants meet nano-/micro-topography of bone scaffolds. Biomedicines, 2021, 9(7): 746

[42] Raja M, Ryu S H, Shanmugharaj A M. Thermal, mechanical and electroactive shape memory properties of polyurethane (PU)/poly (lactic acid) (PLA)/CNT nanocomposites. European Polymer Journal, 2013, 49(11): 3492–3500

[43] Maadani A M, Salahinejad E. Performance comparison of PLA- and PLGA-coated porous bioceramic scaffolds: mechanical, biodegradability, bioactivity, delivery and biocompatibility assessments. Journal of Controlled Release, 2022, 351: 1–7

[44] Bahraminasab M. Challenges on optimization of 3D-printed bone scaffolds. Biomedical Engineering Online, 2020, 19(1): 69

[45] Tafete G A, Thothadri G, Abera M K. A review on carbon nanotube-based composites for electrocatalyst applications. Fullerenes, Nanotubes, and Carbon Nanostructures, 2022, 30(11): 1075–1083

[46] Dixit K, Raichur A, Sinha N. Polymer-coated and nanofiber-reinforced functionally graded bioactive glass scaffolds fabricated using additive manufacturing. IEEE Transactions on Nanobioscience, 2022, 21(3): 380–386

[47] Chen Y, Li X. The utilization of carbon-based nanomaterials in bone tissue regeneration and engineering: respective featured applications and future prospects. Medicine in Novel Technology and Devices, 2022, 16: 100168

[48] Xiao J, Li H, Lu M, et al. Enhancing the interfacial shear strength and tensile strength of carbon fibers through chemical grafting of chitosan and carbon nanotubes. Polymers, 2023, 15(9): 2147

[49] Lan W, Zhang X, Xu M, et al. Carbon nanotube reinforced polyvinyl alcohol/biphasic calcium phosphate scaffold for bone tissue engineering. RSC Advances, 2019, 9(67): 38998–39010

[50] Persaud A, Maus A, Strait L, et al. 3D bioprinting with live cells. Engineered Regeneration, 2022, 3(3): 292–309

[51] Campuzano S, Pelling A E. Scaffolds for 3D cell culture and cellular agriculture applications derived from non-animal sources. Frontiers in Sustainable Food Systems, 2019, 3: 38

[52] Patel D K, Dutta S D, Ganguly K, et al. Enhanced osteogenic potential of unzipped carbon nanotubes for tissue engineering. Journal of Biomedical Materials Research Part A, 2021, 109(10): 1869–1880

[53] Tanaka M, Aoki K, Haniu H, et al. Applications of carbon nanotubes in bone regenerative medicine. Nanomaterials, 2020, 10(4): 659